Journal of Hydrology 496 (2013) 17–30

Contents lists available at SciVerse ScienceDirect

Journal of Hydrology

journal homepage: www.elsevier.com/locate/jhydrol

Channel enlargement in semiarid suburbanizing watersheds: A southern California case study

R.J. Hawley [a,b,1], B.P. Bledsoe [a,*]

[a] Dept. of Civil and Environmental Engineering, Colorado State University, Fort Collins, CO 80523-1372, United States
[b] Sustainable Streams, LLC, 1948 Deer Park Avenue, Louisville, KY 40205, United States

ARTICLE INFO

Article history:
Received 22 November 2012
Received in revised form 6 April 2013
Accepted 4 May 2013
Available online 16 May 2013
This manuscript was handled by Konstantine P. Georgakakos, Editor-in-Chief, with the assistance of Marco Borga, Associate Editor

Keywords:
Channel stability
Grade control
Hydromodification
Sediment transport
Stormwater management
Urbanization

SUMMARY

Semiarid channels exhibit an extreme sensitivity to upstream urban development, particularly in unconfined valleys with unprotected grades. For example, one of our study streams in southern California has increased its cross-sectional area by nearly 14-fold relative to its pre-developed channel form in a watershed that has been only lightly developed (10.4% imperviousness). Multivariate regression models of cross-sectional channel enlargement at 61 sites were highly dependent on the ratio of post- to pre-urban sediment-transport capacity over cumulative duration simulations of 25 yrs (*Lr*), which explained nearly 60% of the variance. The proximity of a channel hard point such as bedrock or artificial grade control was also significant, indicating that channel enlargement increased moving upstream from grade control. The enlargement models point to the importance of balancing the post-developed sediment transport to the pre-developed setting over an entire range of flows rather than a single flow in order to reduce the risk of adverse channel responses to hydromodification. The need for controlling a wide range of flows was underscored by logistic-regression analyses that indicated a high risk of instability in systems with $Lr > 1$, especially for fine-grained systems (i.e., $d_{50} < 16$ mm).

1. Introduction

Watershed urbanization can be a primary driver of hydrologic and geomorphic change in stream channels (i.e., 'hydromodification;' Hammer, 1972; MacRae, 1993) and semiarid systems seem to exhibit an increased sensitivity to this phenomenon (Trimble, 1997; Coleman et al., 2005; Hawley et al., 2012). Previous work in humid temperate systems has linked watershed urbanization to channel enlargement (Hammer, 1972), incision (Booth, 1990), and widening (Galster et al., 2008); however, there is an urgent need for improved understanding of channel response potential in semiarid settings due to the combination of rapid development rates across these regions and stream systems that are inherently dynamic. With sporadic sediment movements (Graf, 1981), extended aggradation/degradation phases (Wolman and Gerson, 1978), and infrequent periods of equilibrium (Bull, 1997), semiarid streams have little natural resistance against unmitigated urbanization. Southern California channels offer a valuable case study because the region includes additional risk factors such as high-relief watersheds with relatively fine-grained bed materials, particularly in unconfined valleys at intermediate and lower portions of the stream network. Moreover, and in contrast to much of the rest of the nation, stormwater controls at the development scale are largely lacking in southern California (based on an extensive field reconnaissance and data-collection campaign). This lack of flow mitigation has consequently amplified flows and durations (Hawley and Bledsoe, 2011), and resulted in rapid and extensive channel enlargement that may be one of the most extreme examples of morphologic channel responses induced by land-use dynamics. For example, an unnamed tributary to the Santa Clara River in north-central Los Angeles County near Acton, California (i.e., 'Acton') has enlarged on the order of 100–1000% over the reach since becoming only lightly developed during the last few years (2.5% impervious area in 2001, 11% in 2006).

1.1. Beyond single-flow analyses: can channel enlargement be predicted using cumulative sediment transport?

The use of single-flow analyses for assessing and managing channel stability has increasingly been brought into question (Graf, 1988; Bull, 1997) because all flows capable of moving sediment

* Corresponding author. Tel.: +1 970 4918410.
E-mail addresses: bob.hawley@sustainablestreams.com (R.J. Hawley), brian.bledsoe@colostate.edu (B.P. Bledsoe).
[1] Tel.: +1 502 7182912.

0022-1694/$ - see front matter © 2013 Elsevier B.V. All rights reserved.
http://dx.doi.org/10.1016/j.jhydrol.2013.05.010

have the potential to affect channel form, and it is the combination of both frequency and magnitude that leads to geomorphic effectiveness (Wolman and Miller, 1960). One of the earliest process-based approaches to managing hydromodification considers the cumulative excess shear stress over all flows capable of transporting the channel-bed material (Santa Clara Valley Urban Runoff Pollution Prevention Program, 2004). The so-called 'effective work index' is computed using binned flows from long-term rainfall runoff simulations in the Hydrologic Engineering Center–Hydrologic Modeling System (HEC–HMS) over cumulative flow durations of 50 yrs.

As an alternative to rainfall–runoff models, Hawley and Bledsoe (2011) developed a regional scaling procedure to model long-term cumulative flow durations and magnitudes as functions of watershed characteristics, such as drainage area, precipitation, and imperviousness. Duration Density Functions (DDFs) estimate cumulative durations for all geomorphically-effective flows in a logarithmically-binned histogram format such that long-term sediment transport can be subsequently estimated.

This paper focuses on applying DDFs and other tools to develop an improved, process-based understanding of channel-response magnitude associated with watershed urbanization. That is, increased flows and durations result in higher sediment-transport potential, culminating in large surpluses of excess energy relative to the pre-developed regime. Models of the corresponding channel enlargement provide managers with tools for predicting changes in channel form in urbanizing watersheds, but more importantly, will lead to informed evaluations of various mitigation strategies to minimize the risk of such channel degradation.

In summary, the objectives of this paper are to address the following questions:

1. Are sediment-transport imbalances between post-developed and pre-developed flow regimes significant in predicting observed channel enlargement, and if so, do sediment imbalances predict enlargement better than previously used surrogates for watershed urbanization such as imperviousness?
2. At what level of sediment imbalance and/or development extent does the risk of channel instability become apparent in semiarid southern California systems?

Resolving these questions could provide watershed managers with a much needed empirical basis for anticipating channel response to varying degrees of development and identifying policies that reduce the risk that channels will cross unacceptable thresholds of enlargement and instability.

2. Methods

Extensive field data were collected and analyzed for this project, guided by independent reviews and state-approved quality-assurance/quality-control (QA/QC) procedures. In general, the modeling approaches used and developed in this paper are designed for broad application in semiarid regions as opposed to high precision along a single reach. Although process-based, the empirical models presented here are more appropriate for quantifying relative extents of change than absolute magnitudes.

In the following sub-sections, we outline the site-selection process and describe how data were collected. We discuss how channel enlargement was quantified based on departures from reference channel form using field measurements coupled with historic aerial photography. Next, computational methods for hydrologic, hydraulic, and sediment-transport processes are covered. Lastly, the analytical and statistical methods are presented, describing how results from the preceding steps were used to develop final models.

2.1. Site selection and channel stability

Pre-developed, developing, and heavily-developed watersheds were targeted to capture a gradient of urbanization relative to the rural setting (Table 1). Sites spanned channel evolution stages from 'stable' single-thread to incising, widening, and braiding (*sensu* Schumm et al., 1984; Hawley et al., 2012). With the understanding that most channels of southern California are inherently dynamic, 'stable' is defined for the purposes of this paper as Channel Evolution Model (CEM) Stages 1 (dynamic equilibrium), B1 (braided dynamic equilibrium), 4 (recovering), and 5 (recovered) from the Schumm et al. (1984) and Hawley et al. (2012) models (Table 2). From field reconnaissance at more than 50 candidate streams, 28 stream reaches were selected for data collection and analysis for this study. We excluded reaches that were reinforced through artificial means due to their inability to freely respond to hydromodification through morphologic adjustment. We also excluded streams with substantial upstream flow regulation (e.g., dams, reservoirs, and large stormwater control facilities) because flow detention in most small watersheds was uncommon at the subdivision scale. The data set was also designed to cover regionally-representative ranges of slope, bed material, channel type/planform, channel evolution stage, valley setting, drainage-basin size, and urbanization extent (Table 2). Stream reaches and watersheds used in the analysis are denoted in Fig. 1.

Along 28 stream reaches (typically 1- to 2-km), 66 geomorphically-distinct sub-reaches or 'sites' were identified for this analysis. Geomorphically-distinct sub-reaches were defined by substantial differences in channel form, contributing drainage area, or valley setting. For example, by collecting several distinct cross sections along a common reach, it was possible to isolate the effects of a downstream channel hard point on channel enlargement.

2.2. GIS and field data collection

All GIS data were acquired from public-domain sources including the USGS; U.S. Department of Agriculture (USDA); National Oceanic and Atmospheric Administration (NOAA), and State of California geospatial clearinghouse (CAL-Atlas). Changes through time were tracked using historical and present-day aerial photography from the USGS and Google Earth, along with historical USGS quadrangle topographic maps. High-resolution historic aerial photography was purchased from the USGS at twelve of our most dynamic study reaches to obtain more precise estimates of historic channel form. Publicly-available low-resolution aerial photography confirmed the lack of historical change at the remaining 16 reaches.

ArcMap software by Environmental Systems Research Institute (ESRI), including extensions such as 'spatial analyst,' was used to optimize GIS measurements where possible. Automated drainage basin delineations were cross-checked with aerial photography, field investigations, and existing shapefiles such as USGS Hydrologic Unit Code (HUC) boundaries and National Hydrography Dataset (NHD) flowlines. Watershed boundaries were independently confirmed by two analysts.

The USGS national impervious raster from 2001 provided an objective way to measure total imperviousness. Because substantial development occurred after 2001 at four study reaches (Acton, Dry, Hasley, and San Timetao), more recent aerial photography was used to quantify more reflective imperviousness estimates for the current extent (Fig. 2).

Bed material was sampled after Bunte and Abt (2001), with 100-particle pebble counts using a half-phi template across equally-spaced sampling frame transects at riffle sections. Sites with more than ~20% sand by volume required sieving and pebble counts. Volumetric gradations (pebble counts using an equally-spaced sampling frame) were composited with distributions by

Table 1
The 66 morphologically-distinct project site (sub-reaches) locations.

Site number	Site identification	Latitude (decimal degrees)	Longitude (decimal degrees)	Site number	Site identification	Latitude (decimal degrees)	Longitude (decimal degrees)	Site number	Site identification	Latitude (decimal degrees)	Longitude (decimal degrees)
1	Santiago_A	33.7153	−117.6468	23	Sanjuan_A	33.5809	−117.5267	45	Santimeta_C	34.0100	−117.1199
2	Hovnanian_A	34.2909	−118.5343	24	Sanjuan_B	33.5828	−117.5236	46	Ltl_Cedar_A	32.6437	−116.8708
3	Hovnanian_B	34.2919	−118.5348	25	Stewart_A	34.4607	−119.2511	47	Perris_1_A	33.8744	−117.1714
4	Ltl_Cedar_B	32.6431	−116.8692	26	SantiagnI_B	33.7092	−117.6142	48	Perris_1_B	33.8749	−117.1719
5	Proctor_A	32.6945	−116.9096	27	Silverado_A	33.7458	−117.6018	49	Perris_1_C	33.8757	−117.1720
6	Proctor_B	32.6954	−116.9092	28	Silverado_B	33.7458	−117.6009	50	Acton_A	34.4923	−118.1662
7	Proctor_TRIB	32.6946	−116.9089	29	Alt_RC2_A	33.9292	−117.1173	51	Acton_B	34.4948	−118.1660
8	Perris_2_A	33.8760	−117.1696	30	Hasley_1_A	34.4672	−118.6648	52	Acton_C	34.4978	−118.1662
9	Perris_2_B	33.8776	−117.1707	31	Hasley_1_B	34.4672	−118.6655	53	Acton_D	34.4983	−118.1659
10	Perris_3_A	33.8775	−117.1685	32	Hasley_2_A	34.4631	−118.6588	54	Borrego_B	33.6725	−117.6906
11	Perris_3_B	33.8799	−117.1695	33	Hasley_2_B	34.4647	−118.6606	55	Borrego_C	33.6737	−117.6873
12	AltPerris_A	33.8752	−117.1478	34	Hasley_2_TRIB	34.4641	−118.6594	56	Borrego_E	33.6794	−117.6819
13	AltPerris_B	33.8759	−117.1473	35	Hicks_B_08	33.7213	−117.7296	57	Challengr_B	34.2397	−118.7727
14	AltPerris_C	33.8767	−117.1469	36	Hicks_C_08	33.7216	−117.7296	58	Pigeon_A	33.9741	−117.2631
15	Dulzura_A	32.6683	−116.8267	37	Hicks_D_08	33.7223	−117.7291	59	Pigeon_B	33.9742	−117.2632
16	Dulzura_B	32.6685	−116.8254	38	Hicks_E_08	33.7237	−117.7276	60	Pigeon_C	33.9822	−117.2699
17	Borrego_D	33.6781	−117.6838	39	Hicks_F_08	33.7246	−117.7270	61	Yucaipa_B	34.0142	−117.0051
18	Topanga_A	34.0474	−118.5798	40	Dry_A	34.2928	−118.7468	62w	Agua_Hedi_A	33.1543	−117.2412
19	Topanga_B	34.0482	−118.5807	41	Dry_B	34.2938	−118.7474	63w	Agua_Hedi_B	33.1540	−117.2397
20	Topanga_C	34.0504	−118.5815	42	Dry_C	34.2946	−118.7479	64w	Agua_Hedi_C	33.1547	−117.2377
21	Challengr_A	34.2400	−118.7754	43	Santimeta_A	34.0073	−117.1197	65w	Sanantoni_A	34.4496	−119.2247
22	Challengr_C	34.2388	−118.7717	44	Santimeta_B	34.0085	−117.1197	66w	Sanantoni_B	34.4496	−119.2247

weight (sieve analyses) using a combination of rigid and flexible procedures (Bunte and Dust, 2008, Pers. Comm.).

Geometric survey procedures were primarily informed by Harrelson et al. (1994). Longitudinal profiles were surveyed at closely-spaced points along the channel thalweg, capturing all vertical and lateral break points. Cross sections were placed at representative riffle sections and surveyed with point spacing that sufficiently captured all significant grade breaks, with particularly high-point density at banks. Total stations were used to collect the geometric data at approximately half of the study sites with lateral and vertical accuracies ranging 1–3 cm. The remaining sites were surveyed using a level-tape method with vertical errors of approximately 0.5 mm per lateral meter (i.e., ~1 cm over a 20-m cross section, see Hawley (2009) for greater detail).

2.3. Channel enlargement relative to reference channel form

Field data were collected during the winter of 2007/2008. Field surveys and assessments of present-day channel stability were used in combination with historic aerial photographs, maps, and testimony of local residents to re-project a representation of the historic channel form (Table 3). Wherever possible, historic channel width was estimated from aerial photographs and depth was based on field indicators (e.g., an artificially-hardened cross section with little signs of incision). Given the uncertainties associated with such inferences, the re-projections were conservative in that they erred on the side of less departure from present-day form. Fig. 3 superimposes four distinct cross sections along the Acton study reach (unnamed tributary to the Santa Clara River near Acton, California) relative to a re-projection of the historic cross section based on field indicators and a series of aerial photographs that depicted a small, single-thread channel with nominal variability between 1948, 1954, 1957, 1974, 1976, 1979, 1986, 1987, and 1989 that was no wider than ~8 m. Channel depth at the downstream-most extent of the reach (protected from incising due to its close proximity to a channel hardpoint) and at the far upstream extent, just upstream of a 3-m headcut (i.e., yet to incise), suggest a pre-response channel depth of ~0.3 m.

Rather than use a cross-sectional area defined by a return-interval flow, we compared measures of the active channel as defined by the cross-sectional area encompassed by the top of bank (of the lowest defined bank). Top of bank was defined *sensu* Osman and Thorne (1988) as the geotechnical location most representative to capture the risk of mass-wasting failure. In channels with little evidence of incision, this often corresponded to the commonly used "bankfull" or "benchfull" surface; however, such agreement would not occur on channels with severe incision. Because differences were generally large and scale-dependent, enlargement was quantified by relative magnitude:

$$Ar = A_{post}/A_{pre} \tag{2.1}$$

where Ar is enlargement expressed as the relative magnitude (m^2/m^2), A_{post} is surveyed cross-sectional area to top of bank (2007/2008), and A_{pre} is best estimate of historic (reference) cross-sectional area.

2.4. Hydrology, hydraulics, and sediment transport

Cumulative flow-duration curves were estimated using a regional regression approach (Hawley and Bledsoe, 2011). The DDF procedure populates long-term durations of histogram-binned flows as functions of physical parameters of the ungauged watersheds and is applicable on drainage areas larger than ~1.3 km^2 for simulation periods of ~25–65 yrs. The disadvantage of the approach, in this case, is that DDFs were constrained by

Table 2
Watershed, valley, and channel attributes.

Site number	*DA* (km^2)	*Imp*[a] (%)	Annual precipitation (mm)	Q_{10} (m^3/s)	*Chnlz* (0 = no, 1 = yes)	*DD* (km/km^2)	*Srf* (%)	S_{valley} (%)	W_{valley} (m)	*VWI*[b] (m/m)	*Confined* (0 = no, 1 = yes)	*Cohesion* (0 = no, 1 = yes)	*Veg* (0 = no, 1 = yes)	d_{50} (mm)	D_{hp}[c] (m)	W_{10}[d] (m)	D_{hp}/W_{10} (m/m)	Planform[e] (S, B, T)	Bedform[f] (C, SP, PB, PR)	CEM[g] (1, 1.5, 2, 3, 4, 5, 2B, 4B, B1, B2)	Stability (S = stable, U = unstable
1	35.09	0.2	594	55.46	0	1.22	46	1.7	230	6.7	0	1	0	22	9600	40.9	235	B	PR	B1	S
2	3.76	1.5	560	7.62	0	1.09	40	4.1	100	7.2	0	0	1	36.7	1100	9.7	113	S	PR	1	S
3	3.74	1.6	560	7.58	0	1.06	40	4.1	45	3.3	0	1	1	16	1100	6.7	164	S	PR	1	S
4	7.21	0.1	413	10.62	0	2.03	36	3.0	120	7.5	0	0	0	20.3	329	28.5	12	B	PB	B1	S
5	11.23	1.5	345	13.59	0	1.64	19	1.6	50	2.8	0	0	0	10.5	4000	23.7	169	B	PB	B1	S
6	5.81	2.7	346	7.69	0	1.46	14	1.6	95	6.8	0	0	0	1.6	4000	18.9	212	B	PB	B1	S
7	3.48	0.0	351	4.99	0	1.60	20	3.1	35	3.1	0	0	0	6.05	4000	15.1	264	B	PB	1	S
8	0.14	1.4	356	0.32	0	1.66	5	4.0	180	55.7	0	0	0	0.9	215	2.9	73	S	PB	1	S
9	0.11	1.8	356	0.26	0	0.28	5	4.0	180	61.4	0	0	0	0.5	447	2.1	209	S	PB	1	S
10	1.46	0.4	356	2.36	0	1.12	9	4.3	400	49.4	0	0	0	0.8	71	22.7	3	B	PB	B1	S
11	1.39	0.3	356	2.26	0	0.96	9	4.3	400	50.4	0	0	0	0.9	400	21.1	19	B	PB	B1	S
12	1.64	0.0	356	2.62	0	0.83	11	0.7	1450	170.9	0	0	0	0.9	200	39.1	5	B	PB	B1	S
13	1.25	0.0	356	2.07	0	1.01	10	0.7	1450	190.5	0	0	0	0.9	300	16.6	18	T	PR	1	S
14	1.24	0.0	356	2.05	0	0.93	10	0.7	1450	191.1	0	0	0	0.8	400	9.8	41	S	PR	1	S
15	70.24	0.3	490	87.33	0	1.55	24	0.8	455	10.8	0	0	0	34.6	3400	33.8	101	S	PR	5	S
16	70.24	0.3	490	87.33	0	1.55	24	0.8	385	9.1	0	0	0	47.7	3400	31.0	110	S	PR	5	S
17	5.76	14.2	454	9.40	1	1.40	26	2.3	230	15.1	0	0	0	45	1121	17.2	65	S	PR	4	S
18	49.80	1.4	561	71.97	0	1.68	31	2.5	55	1.4	1	0	1	87.8	20	25.5	1	S	SP	1	S
19	49.80	1.4	559	71.72	0	1.68	31	2.7	100	2.6	0	0	1	100	100	34.7	3	B	PR	B1	S
20	48.92	1.4	559	70.61	0	1.66	31	9.8	20	0.5	1	0	1	499.5	2	12.0	0	S	SP	1	S
21	7.43	2.3	457	11.79	0	1.67	36	2.0	60	3.6	0	0	1	51.2	885	23.3	38	S	PR	1.5	S
22	7.06	1.4	457	11.27	0	1.69	37	3.0	25	1.5	1	0	1	69.7	146	21.5	7	S	PR	1	S
23	105.24	0.1	533	132.38	0	1.16	33	1.2	350	6.8	0	0	0	34.4	1700	61.1	28	B	PR	B1	S
24	103.67	0.1	533	130.67	0	1.15	33	1.3	40	0.8	1	0	0	61.2	2277	39.4	58	S	SP	1	S
25	4.73	0.1	665	10.61	0	1.67	46	9.6	650	40.4	0	0	0	151.8	200	9.3	22	S	C	1	S
26	16.99	0.0	610	30.18	0	1.39	48	2.9	40	1.5	1	0	0	26.2	13299	12.3	1084	S	SP	1	S
27	21.75	0.0	686	40.91	0	1.24	50	5.5	30	1.0	1	0	1	141.5	3000	12.0	250	S	SP	1	S
28	21.75	0.0	686	40.91	0	1.24	50	5.5	30	1.0	1	0	1	124.3	3085	11.5	269	S	SP	1	S
29	0.16	0.0	356	0.34	0	3.65	17	6.3	90	27.0	0	1	0	0.125	200	1.6	124	S	PR	1	S
30	3.98	4.0	368	5.81	0	1.22	22	2.9	125	10.2	0	0	0	13	100	3.7	27	S	PB	2	U
31	3.98	4.0	369	5.82	0	1.21	22	2.4	125	10.2	0	0	0	3.2	164	7.3	23	S	PB	3	U
32	11.69	4.6	383	15.27	0	1.79	22	3.0	180	9.5	0	1	0	1.6	1700	46.0	37	B	PB	2B	U
33	6.41	5.5	379	8.98	0	1.55	23	3.0	180	12.1	0	1	0	2.6	1950	16.5	118	S	PB	2	U
34	5.05	2.9	391	7.48	0	2.10	21	3.1	180	13.1	0	0	0	1.5	1850	21.7	85	B	PB	2B	U
35	3.87	1.6	422	6.30	0	1.48	27	2.6	60	4.7	0	0	0	0.6	150	6.3	24	S	PB	2	U
36	3.87	1.6	422	6.30	0	1.48	27	2.6	60	4.7	0	0	0	3.8	175	14.9	12	S	PB	3	U
37	3.73	1.6	425	6.13	0	1.47	27	2.6	85	6.8	0	0	0	1.9	283	10.4	27	S	PB	3	U
38	3.58	1.6	429	5.96	0	1.47	27	2.6	85	6.9	0	0	0	1.3	534	13.0	41	S	PB	2	U
39	3.51	1.7	429	5.86	0	1.46	28	2.6	85	6.9	0	0	0	1.3	722	17.8	40	S	PB	2	U
40	3.16	2.2	384	4.90	0	1.77	27	3.0	190	16.8	0	0	0	0.7	33	10.9	3	S	PB	3	U
41	3.09	2.3	384	4.81	0	1.78	27	3.0	130	11.6	0	0	0	0.75	180	10.1	18	S	PB	3	U
42	2.98	2.4	384	4.67	0	1.80	27	3.0	130	11.8	0	0	0	0.8	293	11.6	25	S	PB	3	U
43	1.45	10.5	356	2.35	0	0.53	12	4.6	325	40.3	0	1	0	0.9	4400	3.5	1243	S	PB	3	U
44	1.45	10.5	356	2.35	0	0.43	12	4.6	115	14.2	0	1	0	0.9	4547	7.1	644	S	PB	3	U
45	1.45	10.5	356	2.35	0	0.29	12	4.6	100	12.4	0	1	0	0.9	4751	9.5	499	S	PB	3	U
46	7.21	0.1	413	10.62	0	2.03	36	3.0	130	8.1	0	0	0	28.5	165	9.1	18	S	PB	2	U
47	0.45	2.2	356	0.85	0	1.16	8	2.4	250	49.4	0	1	0	0.8	47	5.0	9	S	PB	1.5	U
48	0.45	2.2	356	0.85	0	0.98	8	2.4	250	49.4	0	0	0	0.8	53	3.6	15	S	PB	2	U

49	0.43	2.3	356	0.82	0	0.77	8	2.4	250	50.2	0	0	0	0.8	28	2.8	10	S	PB	2	U
50	2.02	10.6	229	2.23	0	0.54	18	4.4	160	20.3	0	0	0	4.9	70	16.3	4	B	PB	2B	U
51	1.95	10.8	229	2.17	0	0.40	18	4.4	160	20.5	0	0	0	3.8	425	4.5	94	S	PB	2	U
52	1.87	10.4	229	2.09	0	0.25	19	5.8	130	17.0	0	0	0	5	779	6.5	120	S	PR	3	U
53	1.42	10.9	229	1.65	0	0.26	19	5.8	50	7.3	0	0	0	9.4	866	4.6	187	S	PB	3	U
54	6.99	14.0	440	10.86	1	1.54	23	2.3	240	14.8	0	0	0	1.6	340	39.5	9	B	PB	4B	U
55	6.84	14.3	443	10.70	1	1.49	24	2.8	300	18.6	0	0	0	1	685	20.0	34	S	PB	3	U
56	5.68	14.4	454	9.28	1	1.38	26	2.9	220	14.5	0	0	0	45	20	7.9	3	S	PR	2	U
57	7.32	2.2	457	11.65	0	1.65	36	3.8	25	1.5	1	0	1	3.4	1169	22.7	51	S	PR	2	U
58	6.47	4.6	356	8.62	0	1.27	18	1.6	160	10.9	0	0	0	1.2	300	34.6	9	B	PB	B2	U
59	6.47	4.6	356	8.62	0	1.27	18	1.6	160	10.9	0	0	0	0.9	310	20.6	15	B	PB	B2	U
60	3.53	0.8	356	5.10	0	1.31	19	2.5	100	8.7	0	0	0	1.5	100	7.5	13	S	PR	2	U
61	11.48	2.2	565	20.23	0	1.53	29	3.6	200	9.2	0	0	0	4.8	300	20.3	15	S	PB	4B	U
62w[h]	27.12	26.4	341	28.95	0	1.18	13	0.7	72	2.8	0	0	1	5	50	8.2	6	S	PR	2	U
63w	26.97	26.3	341	28.82	0	1.18	13	0.7	95	3.7	0	1	1	5	225	12.8	18	S	PR	3	U
64w	26.84	26.2	341	28.70	0	1.18	13	0.7	72	2.8	0	1	1	5	416	11.4	37	S	PR	2	U
65w	31.14	0.2	711	57.40	1	1.82	44	1.7	2500	71.7	0	0	0	64	750	29.3	26	S	SP	B2	U
66w	31.14	0.2	711	57.40	1	1.82	44	1.7	2500	71.7	0	0	0	16	750	64.3	12	B	PR	B1	U
max	105.24	26	711	132.38	1.00	3.65	50	10	2500	191.1	1.00	1.00	1.00	499.5	13299	64.3	1243.4				
mean	14.21	4	428	20.15	0.09	1.34	24	3	287	24.0	0.12	0.17	0.20	27.8	1344	17.7	110.1				
min	0.11	0	229	0.26	0.00	0.25	5	1	20	0.5	0.00	0.00	0.00	0.1	2	1.6	0.2				
std. dev.	22.71	6	115	29.78	0.29	0.54	12	2	493	39.7	0.33	0.38	0.40	68.3	2260	13.6	220.2				
skew	2.59	2.17	0.81	2.26	2.91	0.68	0.45	1.52	3.46	3.19	2.38	1.83	1.56	5.43	3.30	1.43	3.82				

[a] Watershed imperviousness from the 2001 U.S. Geological Survey (USGS) national impervious raster except at four study reaches (Acton (2006), Dry (2007), Hasley (2006), and San Timetao (2008)) where substantial development occurred after 2001 and more recent public domain (USGS) aerial photography was used in a geographic information system (GIS) to develop more reflective values from the period of our field data collection.

[b] VWI (Valley Width Index) developed after Bledsoe et al. (2012) as the ratio of the available valley width to the reference channel width. VWI < 2 were considered "confined" valleys and VWI > 2 were considered unconfined.

[c] D_{hp} defined as distance to nearest downstream hard point such as natural bedrock or artificial grade control.

[d] W_{10} defined as channel top width at 10-yr flow.

[e] Planform categorized as Single thread, Braided, or Transitional. Note that sinuosities of all channels were relatively low such that single-thread channels were typically 'straight' rather than 'meandering'.

[f] Bedform categorized as Cascade, Step Pool, Plane Bed, or Pool Riffle after Montgomery and Buffington (1997).

[g] CEM stage categorized after Hawley et al. (2012) developed for channel evolution in response to urbanization in semiarid settings.

[h] Sites 62w through 66w were withheld from specific models presented in this paper due to the poor distribution of their primary drivers in this data set, including dense bank vegetation (Agua Hedionda) and historic channelization (San Antonio).

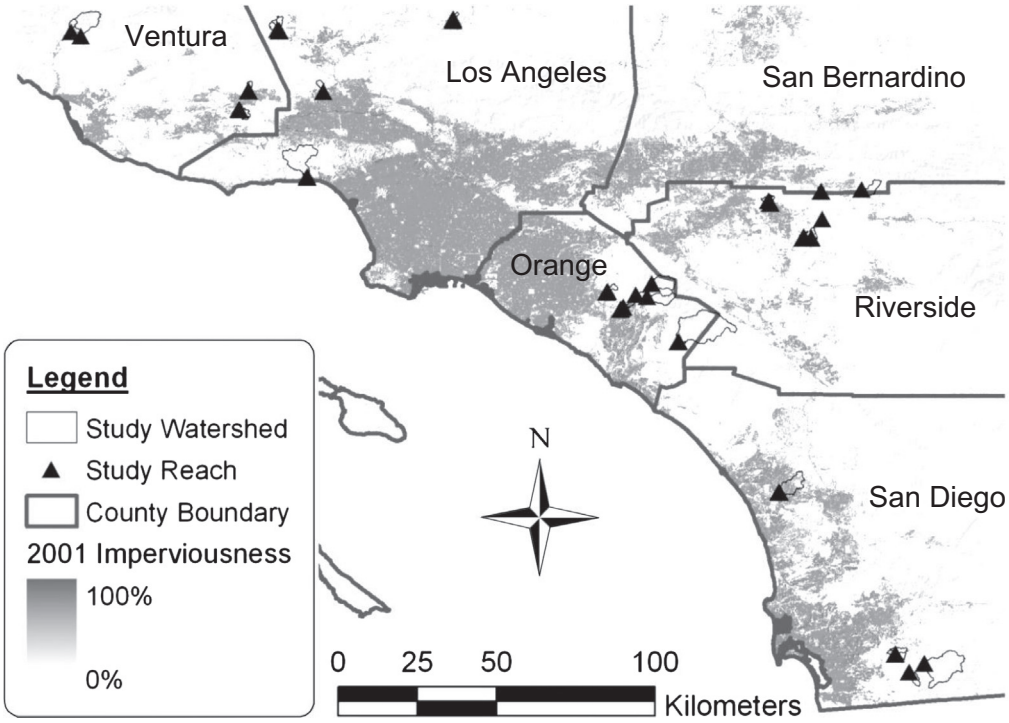

Fig. 1. Study area overview and watershed/reach locations with superimposed county boundaries and impervious cover in 2001 (many of the watersheds are so small that the reach symbol masks their watershed boundary due to the necessary scale for publication).

mean-daily flows rather than more frequent intervals such as hourly or 15-min data, which can adversely affect long-term sediment yields. For example, Watson et al. (1997) reported 50% lower yields using 24-h flows relative to 15-min intervals in small (<1000 km^2) flashy systems in the Yazoo River Basin of Mississippi.

The type and number of histogram bins also affect the sediment-distribution curve (Hey, 1997; Soar, 2000; Holmquist-Johnson, 2002; Raff et al., 2004; Bledsoe et al., 2007). The limiting factor is to ensure a relatively continuous flow frequency such that no bins are populated by zero days of occurrence (Biedenharn et al., 2000, 2001), and Hawley and Bledsoe (2011) found the extremely flashy regimes of southern California to be best represented by 25 logarithmically-distributed bins. The likely underestimate of sediment transport resulting from daily flow bias was partially addressed by fitting DDFs to the arithmetic-bin centroid rather than the logarithmic, creating a slightly-higher representative flow for each bin (i.e., 3.29 vs. 3.23 m^3/s for bin 25 at Borrego_B under the post-developed regime).

The DDFs have particular utility to this study in that they were calibrated with regional data with relatively high accuracies (R^2 0.7–0.9). They also offer an objective way to estimate the amplified flows and durations resulting from urbanization using measures of total impervious area (TIA). In this region, TIA tended to be fairly representative of hydrologically-connected impervious area due to little flow control at the subdivision scale to date. Finally, it is important to note that the models are used in a relative way, comparing post-developed/pre-developed scenarios rather than absolute estimates of yield. That is, the inherent errors of the models are unbiased in affecting both scenarios such that results are meaningful in terms of relative imbalances.

DDF 25-yr simulations were performed for post-developed and pre-developed flow regime scenarios by using the most current impervious extent relative to no impervious cover. After pre-developed/post-developed DDFs were estimated, hydraulics and sediment transport were determined for the centroid of each flow bin based on surveyed present-day geometry. Present-day geometry was used for both pre- and post-developed scenarios because of the uncertainties associated with the projected pre-developed channel bed geometry (in both cross-section and longitudinal profile), given that historic aerials could only reasonably estimate channel width. This approach may have over-predicted sediment-transport capacity of the pre-developed channel form in cases of entrenched geometry (e.g., CEM Stage 2), and may have under-predicted cumulative sediment-transport capacity in reaches that were overly widened with flattened slopes (e.g., CEM Stage 4). This is discussed in greater detail in Section 4.

Hydraulic calculations were simplified by using at-a-station hydraulic-geometry relationships developed using present-day geometry at each site after Buhman et al. (2002), such that water surface width, area, and hydraulic radius could be easily and accurately estimated by the depth of a given flow. This included power functions for area and hydraulic radius (R^2 commonly approaching 1.00), and a predictor of top width based on power, linear, logarithmic, or exponential models that provided the best fit at a given site (R^2 typically ranging 0.97–0.99), and resulted in highly-efficient and accurate hydraulic calculations for each of the 25 bin flow centroids at every site.

Normal depth at the respective flows was iteratively solved via the Manning equation and hydraulic radius power function based on estimates of Manning n made in the field after Chow (1959). Sediment-transport capacity was estimated for each site based on hydraulics of each bin flow. All but one site had a median particle diameter (d_{50}) greater than 0.5 mm, making the Meyer-Peter and Müller (1948) adequate for this analysis. The volumetric unit bedload form of the equation (Chien, 1956; Julien, 1998) is presented below with the recently corrected parameters of Wong and Parker (2006):

$$q_{bv} = 3.97 * (\tau_* - \tau_{*c})^{1.6} * \{(G-1)gd_s^3\}^{0.5} \quad (2.2)$$

where q_{bv} is unit bedload discharge by volume; τ_* is dimensionless shear stress, approximated for gradually-varied flow as $\tau_* = RS_f/$

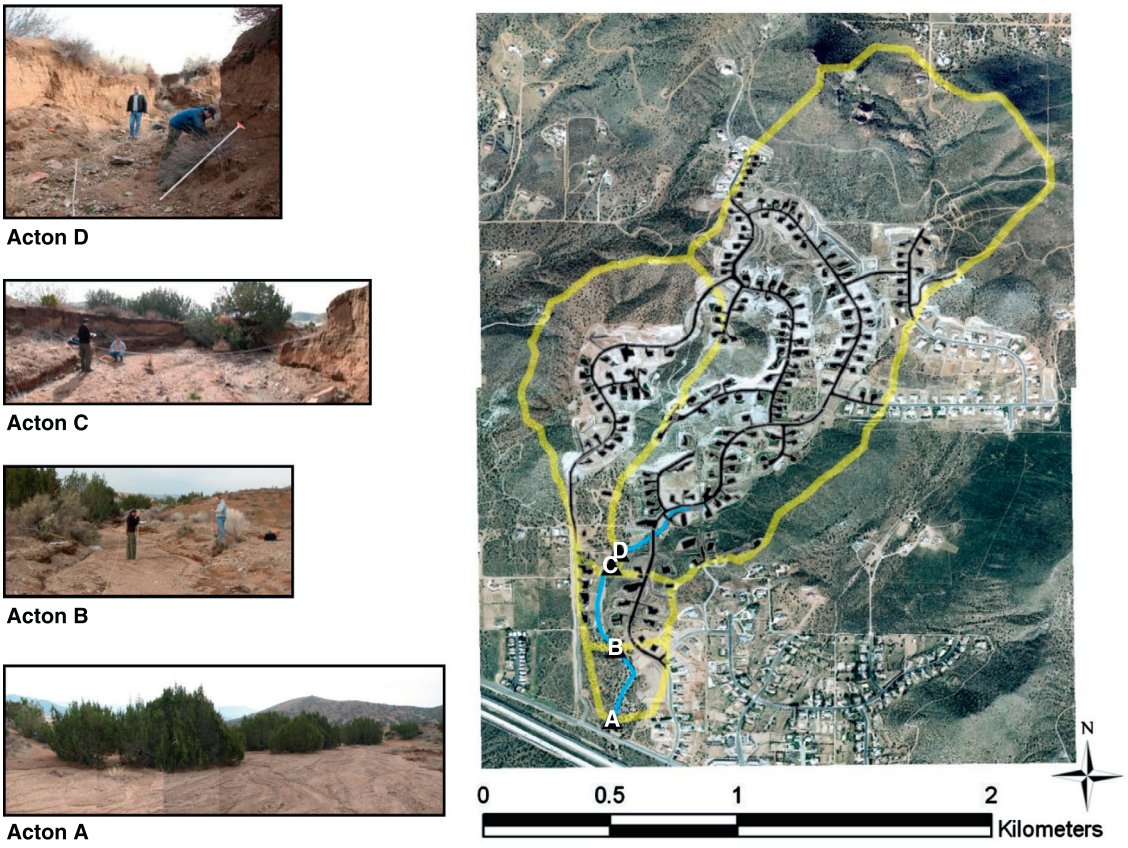

Fig. 2. Aerial photograph (2006) of Acton watershed (north-central Los Angeles County) and superimposed impervious cover, watershed boundaries, and study sites (with photographs by D. Dust).

$\{(G-1)^{*} d_s\}$, where R = hydraulic radius and the friction slope (S_f) may be approximated by the bed slope; τ_{*c} is Shields parameter for incipient motion, calibrated to this equation as $\tau_{*c} = 0.047$ for high rates of transport; G is specific gravity of sediment; g is acceleration of gravity; and d_s is sediment particle diameter, applied in our case for the median particle (d_{50}).

Unit bedload rates were calculated for each bin ($q_{b\text{-}bin}$) and integrated across the respective channel width and over the number of flow days to estimate time-integrated bedload capacity for a bin ($L_{b\text{-}bin}$) during the simulation period. Summing the bedload from each bin provided a cumulative estimate of bedload yield for the 25-yr simulation. Finally, bedload estimates from the post-developed and pre-developed simulations were compared using their direct ratio ($Lr = L_{post}/L_{pre}$). It is important to note that all of the sediment analyses are based on estimates of sediment-transport capacity, and are independent of actual sediment supply. The approach is justified by the fact that we are not attempting to develop accurate estimates of sediment yield; rather, we use sediment-transport capacity as a surrogate for the cumulative erosive power of the flow regime expressed on the given channel setting. Because we use ratios that compare post-developed sediment-transport capacity to pre-developed, the only potential caveat for such an approach would be in cases where urbanization affected the sediment supply, particularly in cases where it may reduce the supply of coarse sediment. This is discussed in greater detail in Section 4.1.

2.5. Analytical and statistical methods

Despite the inclusion of several physical factors in the models (e.g., slope, width, grain size, flow and durations, etc.), we hypothesized that sediment-transport imbalances would be highly significant in explaining changes in channel form in both continuous (i.e., regression models of 'enlargement') and threshold models (i.e., logistic regression models of stable vs. unstable CEM stages). In addition, we tested an array of competing hydrogeomorphic variables for statistical significance to identify potential 'risk factors' for channel enlargement. Many of the variables were log-transformed to make their distributions more normal. We used forward, backward, and best-subset selection to arrive at the best-performing models. Model performance was assessed based on high significance of individual variables (typically $p < 0.05$), high adjusted R^2 and/or minimum Mallow's Cp, physical interpretability, and standard diagnostics.

Logistic-regression analysis can be a valuable tool when interested in the probability of a binary state (i.e., unstable vs. stable). Logistic-regression models were developed using maximum likelihood techniques that optimize parameters to maximize correct classification of the observed data. Performance was assessed using rates of correct classification, along with p-values associated with the χ^2 statistic, which compares the likelihood of the fitted model to a null model in which all parameters are zero. We used the Statistical Analysis Software (SAS®) software package for all statistical analyses.

3. Results

The 25-yr simulations of cumulative sediment-transport capacity, based on cumulative duration flow histograms after Hawley and Bledsoe (2011), quantified large differences in both the duration of erosive flows and their cumulative sediment-transport capacity. Fig. 4 depicts post- vs. pre-urban differences in a

Table 3
Channel enlargement attributes.

Site number	Lr^j (m^3/m^3)	A_{bf} post-developed (m^2)	W_{bf} post-developed (m)	A_{bf} pre-developed (m^2)	W_{bf} pre-developed (m)	Ar^j (m^2/m^2)	Wr^j (m/m)	Pre-development reference (AP = aerial photograph, FI = field indicators (yr))
1	1.02	64.2	75.4	64.2	75.4	1.00	1.00	AP (1947, 1982)
2	1.16	14.8	16.5	14.8	16.5	1.00	1.00	AP (1982)
3	1.18	7.7	8.1	7.7	8.1	1.00	1.00	AP (1982)
4	1.01	15.3	46.0	15.1	46.0	1.01	1.00	FI & AP (1982)
5	1.15	34.0	18.4	34.0	18.4	1.00	1.00	FI
6	1.35	4.8	14.6	4.8	14.6	1.00	1.00	FI
7	1.00	1.9	20.7	1.9	20.7	1.00	1.00	FI
8	1.23	0.8	5.2	0.8	5.2	1.00	1.00	FI
9	1.31	0.6	4.0	0.6	4.0	1.00	1.00	FI
10	1.05	17.5	57.4	17.5	57.4	1.00	1.00	FI
11	1.04	27.1	65.1	27.1	65.1	1.00	1.00	FI
12	1.00	7.2	48.7	7.2	48.7	1.00	1.00	FI
13	1.00	4.0	16.3	4.0	16.3	1.00	1.00	FI
14	1.00	5.3	13.0	3.8	13.0	1.40	1.00	FI
15	1.02	23.7	25.4	15.9	17.9	1.49	1.41	FI & AP (1971)
16	1.02	22.3	22.1	15.9	17.9	1.40	1.24	FI & AP (1971)
17	3.62	160.8	29.5	23.9	14.0	6.72	2.11	FI & AP (1952)
18	1.09	20.1	23.9	20.1	23.9	1.00	1.00	FI & AP (1989)
19	1.08	50.5	42.3	25.1	29.6	2.01	1.43	FI & AP (1989)
20	1.09	37.2	17.5	37.2	17.2	1.00	1.02	FI & AP (1989)
21	1.22	3.3	3.3	2.1	6.3	1.58	0.52	FI & AP (1982, 1989)
22	1.13	2.6	5.2	2.6	5.2	1.00	1.00	FI & AP (1982, 1989)
23	1.01	8.8	41.5	8.8	41.5	1.00	1.00	AP 1982
24	1.01	19.9	20.7	19.9	20.7	1.00	1.00	AP 1982
25	1.01	3.3	6.5	3.3	6.5	1.00	1.00	FI & AP (1963)
26	1.00	8.2	6.0	8.2	6.0	1.00	1.00	FI
27	1.00	8.4	8.9	8.4	8.9	1.00	1.00	FI
28	1.00	5.2	7.2	5.2	7.2	1.00	1.00	FI
29	1.00	6.6	8.0	6.6	8.0	1.00	1.00	FI
30	1.53	4.1	4.3	2.3	3.9	1.84	1.11	FI & AP (1994)
31	1.57	7.8	8.3	2.3	3.9	3.45	2.15	FI & AP (1994)
32	1.60	40.3	68.4	16.3	25.2	2.47	2.71	FI & AP (1994)
33	1.78	59.3	23.7	16.3	23.7	3.63	1.00	FI & AP (1994)
34	1.37	12.7	24.4	4.2	8.1	3.00	3.00	FI & AP (1989)
35	1.20	1.9	3.7	1.6	3.7	1.22	1.00	FI & AP (1982)
36	1.20	2.0	6.4	1.6	14.9	1.28	0.43	FI & AP (1982)
37	1.21	3.8	6.0	1.6	6.3	2.37	0.95	FI & AP (1982)
38	1.21	2.3	3.1	1.6	14.3	1.45	0.22	FI & AP (1982)
39	1.21	4.2	7.3	1.6	12.5	2.65	0.58	FI & AP (1982)
40	1.31	21.2	27.9	8.4	12.0	2.52	2.33	FI & AP (1989)
41	1.31	22.5	21.1	8.4	5.0	2.68	4.23	FI & AP (1989)
42	1.31	25.0	14.1	8.4	10.0	2.98	1.41	FI & AP (1989)
43	3.78	34.9	10.9	10.0	5.0	3.49	2.18	FI & AP (1989)
44	3.76	26.6	13.9	6.5	6.5	4.09	2.14	FI & AP (1989)
45	3.68	13.1	12.8	3.5	5.0	3.73	2.56	FI & AP (1989)
46	1.01	11.5	12.4	5.2	46.0	2.20	0.27	FI & AP (1982)
47	1.35	5.3	9.3	3.5	9.6	1.51	0.97	FI
48	1.36	5.3	11.7	4.0	11.7	1.33	1.00	FI
49	1.36	4.9	6.1	4.2	6.2	1.18	0.98	FI
50	3.72	3.8	18.5	1.7	8.0	2.24	2.32	FI & AP (1989)
51	3.74	3.8	7.0	1.7	8.0	2.23	0.88	FI & AP (1989)
52	3.59	23.5	10.7	1.7	8.0	13.68	1.34	FI & AP (1989)
53	3.83	16.9	6.2	1.7	8.0	9.85	0.77	FI & AP (1989)
54	4.43	144.6	104.6	23.9	14.0	6.04	7.47	FI & AP (1952)

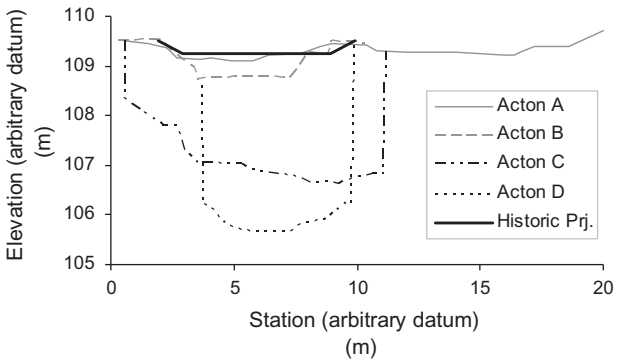

Fig. 3. Superimposed cross sections at Acton relative to projected reference form via historic aerial photography and present-day field indicators. (Field indicators include depth at Acton A and pre-incision depth at Acton B, combined with reach-averaged historic channel width from aerial photography (1948–1989).)

lightly-developed (10.4% imperviousness in 2006) basin in north-central Los Angeles County near Acton, California (i.e., "Acton"). The highly-susceptible bed material (d_{50} = 5 mm) in a relatively steep (5.8% valley slope), unconfined valley setting showed little resistance to the post-developed flow regime relative to the pre-developed setting. The resulting sediment-transport load ratio (Lr) of 3.6 indicates that the cumulative sediment-transport capacity increased approximately 360% over the 25-yr period. Combined with the relatively-unprotected grade (closest downstream hard point was ca. 800 m), this increase in cumulative sediment-transport capacity has resulted in enlargement of nearly fourteen times the pre-developed reference morphology (Table 1, Fig. 3). In a more-detailed time-series analysis of the same stream, Hawley et al. (2012) documented that channel planform and top width remained relatively unchanged as tracked by a series of aerial photographs (1948, 1954, 1957, 1974, 1976, 1979, 1986, 1987, and 1989), with the watershed remaining undeveloped through at least that period (2.3% impervious in 2001, 10.6% in 2006). Recent aerial photography (2006), testimony of local residents, and field data collection all suggest that the measured channel enlargement corresponded to this more recent period of watershed development.

Multivariate regression models of channel enlargement were highly dependent on development extent and corresponding increases in sediment-transport capacity relative to the pre-developed regime. The downstream distance to a channel hard point was also strongly correlated to channel enlargement, especially when standardized by channel width, indicating that cross-sectional area increased moving upstream from a bedrock or artificial grade control. A necessary caveat with the application of the hard-point variable was that it was treated as zero in systems where headcuts were not occurring—that is, channels in relative equilibrium would clearly not be expected to become larger with decreasing catchment size. In our relatively-large data set, the threshold corresponding to the presence/absence of headcutting varied based on substrate type, and was roughly quantified as a sediment-transport ratio greater than ~1.20 in systems with a median grain size >16 mm, and $Lr \sim 1.05$ when $d_{50} < 16$ mm.

Multivariate regression models based on forward selection identified large distances from grade control, high-development extent and corresponding sediment-transport capacity load ratio, and historic channelization as the most influential factors in predicting channel enlargement at all 66 study sites (Table 4). When withholding two reaches where enlargement could be predominantly explained by historic channelization (San Antonio), and where enlargement had been kept somewhat in check with

55	4.42	104.9	27.9	23.9	14.0	4.38	1.99	FI & AP (1952)
56	3.86	36.2	18.4	23.9	14.0	1.51	1.31	FI & AP (1952)
57	1.25	3.7	2.0	2.4	6.0	1.55	0.33	FI & AP (1982, 1989)
58	1.65	4.3	13.9	2.7	13.9	1.61	1.00	FI & AP (1966, 1980, 1989)
59	1.64	5.0	15.5	3.4	15.5	1.45	1.00	FI & AP (1966, 1980, 1989)
60	1.09	5.8	6.9	5.0	6.9	1.16	1.00	FI & AP (1966, 1980, 1989)
61	1.19	66.1	29.6	26.2	26.8	2.52	1.11	AP (1952, 1966, 1969, 1975, 1982, 1983, 1989)
62w[k]	9.37	17.0	15.6	9.2	9.6	1.85	1.62	FI
63w	9.29	19.5	11.8	9.2	9.6	2.12	1.23	FI
64w	9.21	24.4	14.9	9.2	9.6	2.66	1.55	FI
65w	1.01	121.1	65.6	15.0	15.0	8.07	4.38	AP (1947, 1967, 1979, 1982, 1985, 1989)
66w	1.01	115.4	65.4	15.0	15.0	7.69	4.36	AP (1947, 1967, 1979, 1982, 1985, 1989)
max	9.37	160.8	104.6	64.2	75.4	13.68	7.47	
mean	2.00	24.4	21.3	10.5	16.3	2.38	1.45	
min	1.00	0.6	2.0	0.6	3.7	1.00	0.22	
std. dev.	1.90	34.4	20.8	11.1	14.9	2.32	1.14	
skew	2.79	2.50	1.94	2.26	2.23	2.89	3.08	

[i] Lr defined as the sediment-transport capacity load ratio between 25-yr post-developed and pre-developed DDF simulations, $Lr = L_{post}/L_{pre}$.
[j] Ar and Wr defined as ratios of the bankfull cross-sectional area and top width, respectively, where they measure the ratio of the post-developed value to the pre-developed or reference value.
[k] Sites 62w through 66w were withheld from specific models presented in this paper due to the poor distribution of their primary drivers in this data set, including dense bank vegetation (Agua Hedionda) and historic channelization (San Antonio).

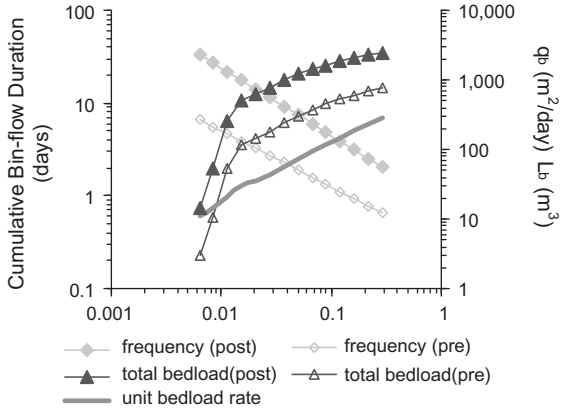

Fig. 4. 25-yr DDF and cumulative sediment-transport simulations at Acton C (10.4% impervious in 2006) using post-developed (post) and pre-developed (pre) flow regimes. q_b is the unit bedload discharge by volume and L_b is the total bedload (i.e., q_b integrated over the channel width and multiplied by the corresponding bin duration).

atypically-dense bank vegetation (Agua Hedionda), both of which were clear outliers (Fig. 5), nearly 60% of the variance in channel enlargement could be explained by *Lr* or watershed imperviousness (Tables 4 and 5).

The models with the screened data ($n = 61$) also reported a higher partial R^2 for downstream hard-point distance (Table 4) when compared to the models that included the outliers ($n = 66$). In contrast, the proportion of variance explained by historic channelization dropped substantially between the two model scenarios, indicating that the significance of channelization in the full model was clearly dependent on data from a single reach (San Antonio), which was otherwise an outlier within this data set. Withholding the statistical outlier of Agua Hedionda was further supported by subsequent field surveys, which showed that the dense vegetation had only postponed channel enlargement—Agua_Hedi_C more than doubled in cross-sectional area between 2007 and 2011.

Therefore, it should be noted that although well-fit, the adjusted R^2 values are probably overly optimistic in application, and the models should be tempered with judgment based on field-based observations of local conditions. For example, the data set does not encompass enough sites with historic channelization to adequately predict the legacy effects of channel relocation. The models in this paper also exclude sites with substantial upstream flow control, such that sites downstream of major reservoirs or stormwater detention structures may not be anticipated to show similar increases in cross-sectional area. Furthermore, some of the channel enlargement over the study period may have been partially attributable to El Nino years that were particularly strong in 1983 and 1998 (Smith and Sardeshmukh, 2000), which are also evident in the precipitation records: 1978, 1983, 1998, and 2005 had rainfall volumes that were 80–130% above the long-term average (Hawley and Bledsoe, 2011).

Based on multivariate regression modeling using forward, backward, and best-subset variable selection, binary variables for valley confinement and bank cohesion, along with continuous variables of drainage density, and average surface slope of the watershed all showed significance at the $p < 0.05$ level, particularly when used in combination with *Lr*, *Imp*, or D_{hp}/W_{10} (Table 4). However, the most powerful predictors of channel enlargement in this data set were watershed imperviousness, corresponding increases in sediment-transport capacity, and the downstream distance to a channel hard point.

Table 4
Channel enlargement risk factors.

Variable	Description	Qualitative influence	Partial R^2 [a]	
			$n = 66$	$n = 61$ [b]
Lr	Sediment-transport capacity load ratio between 25-yr post-developed and pre-developed DDF simulations: L_{post}/L_{pre} (m^3/m^3)	+	.28	.58
Imp	Total impervious area as fraction of total drainage area (m^2/m^2)	+	.21	.56
D_{hp}/W_{10}	Downstream distance to nearest 'hard point' (bedrock or artificial) scaled by top width at 10-yr flow (m/m), **term goes to 0 if Lr < 1.20 for d_{50} > 16 mm OR if Lr < 1.05 for d_{50} < 16 mm**	+	.32	.34
Chnlz	Binary variable representing historic channelization along reach (0 = unchannelized, 1 = channelized)	+	.20	.01
Confined	Binary variable representing valley confinement as defined as a VWI threshold of 2 (0 = VWI > 2), 1 = VWI < 2)	−	.01	.02
Srf	Average surface slope of watershed (m/m)	+	.02	.01
DD	Drainage density: total stream length via NHD / total drainage area (km/km^2)	+	.01	.01
Veg	Binary variable representing bank vegetation (0 = poor, 1 = dense)	−	.03	.01
Cohesion	Binary variable representing relative bank cohesion (0 = low, 1 = high)	−	.01	.01

[a] Typical partial R^2 based on model forward selection.
[b] Withheld stream reaches where enlargement was primarily driven by historic channelization (San Antonio) or kept artificially low due to dense vegetation (Agua Hedionda); both factors were poorly distributed in our data set.

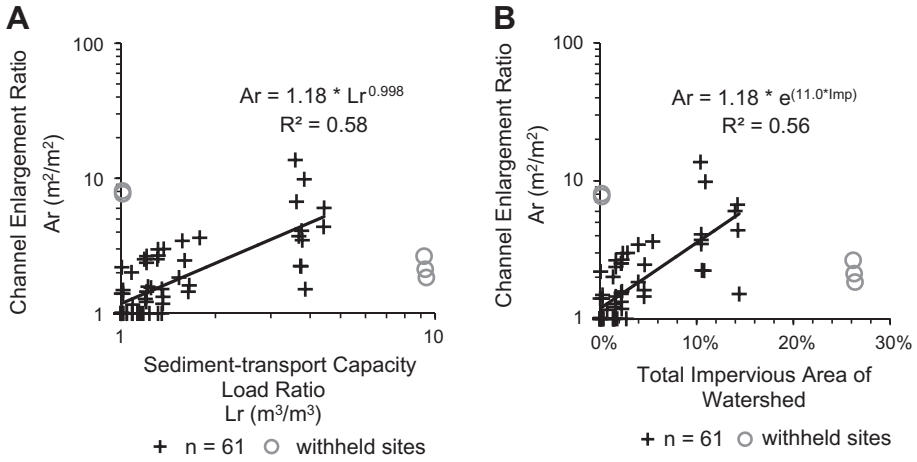

Fig. 5. Cross-sectional channel enlargement as bivariate functions (based on the withholding of two stream reaches where enlargement was primarily driven by historic channelization (San Antonio) or kept artificially low due to dense vegetation (Agua Hedionda); both factors were poorly distributed in our data set) of: (A) *Lr*, sediment-transport capacity load ratio, and (B) watershed imperviousness, indicating that channel enlargement increases with increasing watershed development and sediment-transport imbalances.

Table 5
Enlargement models and performance.

	Adjusted R^2	*p*-Value exceptions
Enlargement function, $n = 66$		
$Ar = 0.757 * Lr^{0.433} * (D_{hp}/W_{10})^{0.133} * e^{(1.65*Srf)} * e^{(-0.373*Veg)} * e^{(0.613*Chnlz)}$	0.58	
Enlargement functions after systematic screening,[a] $n = 61$		
$Ar = 0.845 * Lr^{0.831} * (D_{hp}/W_{10})^{0.0751} * e^{(1.11*Srf)} * e^{(-0.246*Veg)}$	0.61	$Veg = 0.14$, $Srf = 0.05$
$Ar = 0.863 * e^{(8.83*Imp)} * (D_{hp}/W_{10})^{0.0862} * e^{(0.987*Srf)} * e^{(-0.252*Veg)}$	0.60	$Veg = 0.13$, $Srf = 0.09$
$Ar = 0.885 * Lr^{0.846} * (D_{hp}/W_{10})^{0.0770} * e^{(0.715*Srf)}$	0.60	$Srf = 0.16$
$Ar = 0.906 * e^{(8.98*Imp)} * (D_{hp}/W_{10})^{0.0885} * e^{(0.575*Srf)}$	0.59	$Srf = 0.26$
$Ar = 0.868 * Lr^{0.904} * (D_{hp}/W_{10})^{0.0650} * e^{(0.149*DD)}$	0.60	$DD = 0.17$
$Ar = 1.09 * Lr^{0.836} * (D_{hp}/W_{10})^{0.0614}$	0.59	
$Ar = 1.07 * e^{(8.97*Imp)} * (D_{hp}/W_{10})^{0.0750}$	0.59	
$Ar = 1.18 * Lr^{0.998}$	0.57	
$Ar = 1.18 * e^{(11.0*Imp)}$	0.55	

[a] Withheld stream reaches where enlargement was primarily driven by historic channelization (San Antonio) or kept artificially low due to dense vegetation (Agua Hedionda); both factors were poorly distributed in our data set.

Furthermore, when combined with grain size, *Lr* provided stratification of channel stability using logistic-regression analysis, in which models ($p < 0.0001$) and individual terms were significant ($p < 0.05$). As seen in Fig. 6A, sand systems have essentially no capacity to absorb changes in sediment-transport capacity without proportional responses in channel form. Channels with beds of fine to medium gravel ($d_{50} \sim 2$–16 mm) also appear to be extremely sensitive to seemingly nominal sediment balances

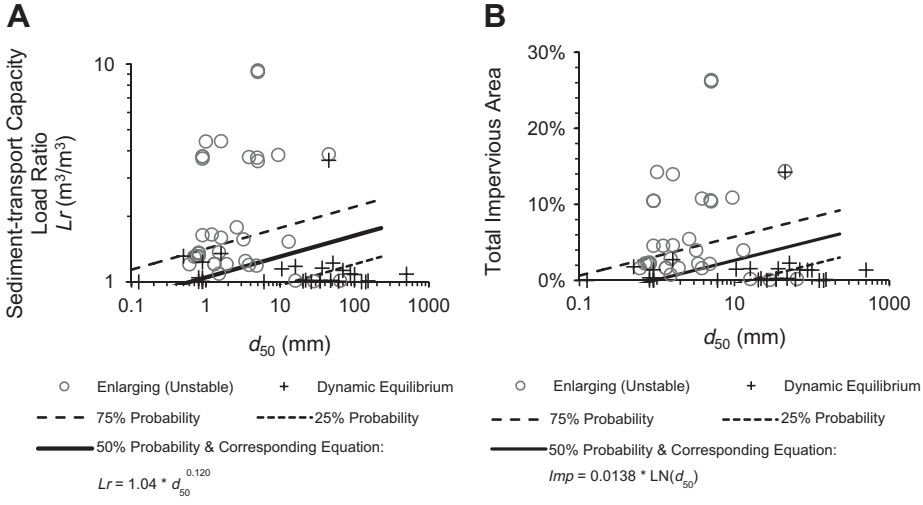

Fig. 6. Multivariate logistic-regression analysis of dynamic equilibrium vs. enlarging (unstable) systems as a function of median grain size and (A) *Lr*, sediment-transport capacity load ratio, and (B) total impervious area.

(i.e., $Lr \sim 1.01$–1.05). Some capacity to withstand perturbations in erosive energy is apparent in the coarse-gravel range (i.e., $d_{50} \sim 16$–64 mm); however, substantial resistance does not become apparent until reaching a d_{50} greater than 64 mm.

When using watershed imperviousness in the place of *Lr* (Fig. 6B), model shape and significance were nearly identical. All systems showed very little resistance above ca. 5% impervious area. The single outlier in both figures is Borrego_D, a site that has enlarged by nearly sevenfold relative to its pre-developed reference channel, but has recently begun to restabilize (CEM Stage 4 after Schumm et al. (1984)) due to the substantial coarsening of its bed material (d_{50} 1 mm → 45 mm), slope reduction, and increased channel width.

4. Discussion

A central conclusion from this study is that many semiarid channels are extremely sensitive to hydromodification. We observed very few channels in unconfined valleys that could obtain single- or multi-thread stability—even at relatively-low levels of imperviousness—without some measure of artificial control. Small degrees of development and associated sediment imbalances can create significant responses in channel form. The sediment-transport capacity ratio explained ca. 60% of the variance in enlargement in primarily unmitigated urban systems. Based on the $Ar = 1.18\ Lr^{1.0}$ model (Table 5), for every increase in the cumulative sediment-transport ratio there was a nearly equal increase in cross-sectional area at the average study site. Given that 40% of the variability remained unexplained with this simple linear model, the 'true' model may be nonlinear and could better explain the more exponential enlargement observed at some sites, particularly those that were far removed from grade control.

A necessary caveat with the models is that they do not account for responses in pre-developed systems attributable to headcutting from below, channelization, or other legacy effects. That is, large responses were observed in pre-developed and even coarse systems that were not attributable to upstream urbanization (i.e., matching *Lr* on a new development would not ensure stability in channelized systems). Furthermore, the models may underestimate potential enlargement values in that many of the streams used in the analysis are still actively adjusting and could become even larger. The fact that present-day geometry was used to model sediment-transport capacity, as opposed to pre-developed geometry or morphology that evolved through time, possibly overestimated sediment transport in entrenched systems (CEM Stage 2) and underestimated capacity in overly-widened systems with flattened slopes (CEM Stages 3 and 4). These countervailing cases may partially explain the relatively large, but equally-distributed variance about the mean trend in Fig. 5A. As an example, using the historic projection geometry at Acton with a well-connected floodplain (Fig. 3), the load ratio between the post-developed and pre-developed 25-yr DDF simulations was 3.53, compared to a load ratio that ranged 3.59–3.83 using the present-day surveyed geometries of the four study sites, with an average of 3.72 (a 5% difference).

In summary, these results demonstrate the utility of multivariate regression models in predicting channel response to hydromodification. More complex modeling approaches, such as continuous hydrologic simulations with coupled mobile boundary models may provide more-detailed time-series adjustments in channel form. Furthermore, artificial neural networks (ANNs) could potentially outperform the simple regression models that were undertaken in this analysis. Despite the limitations of the regression relationships developed in the present study with respect to nonlinear and threshold responses, these models explained 55–61% of the observed variance in channel enlargement using only one to five predictor variables. The utility of our simplest regression model is perhaps most compelling: if the cumulative sediment-transport capacity is increased relative to the pre-development regime, managers can expect, on average, proportional magnitudes of channel enlargement for similar stream types in the study region (Fig. 5).

4.1. Mitigation implications

In watersheds where urbanization does not adversely impact the supply of coarse sediment, channel stability is particularly dependent on the erosive portion of the flow regime; therefore, stormwater management should explicitly focus on the magnitude and duration of all flows above the critical flow for entrainment of the channel-bed material. In many southern California systems, this is essentially all flows which clearly impose practical limitations such as minimum pipe sizes for retention/detention outfalls; however, investments might be made more cost effective by incorporating the relative sensitivity of the receiving channel. For example, mitigation design targets could be based on risk categories that incorporate key predictors of channel response such as bed material resistance and grade-control spacing (Bledsoe et al., 2012), similar to the County of San Diego's (2011) stormwater permit.

Managers might offer a range of site-specific mitigation options that are acceptable to local stakeholders and attempt to match the pre-developed cumulative sediment-transport potential to the extent practicable. Strategies could include a staggered detention facility (*sensu* Distributed Runoff Control; MacRae, 1991, 1993, 1997) that releases flows at incremental rates above a minimum retention/infiltration requirement, entraining bed material more regularly, and at flows that more closely resemble the pre-developed flow regime. Implementing such a scheme in conjunction with low impact development (LID) technologies that promote on-site water reuse, infiltration, and slow runoff at the source would likely prove to be more beneficial for both stability and ecologic function. Until the efficacy of such an approach in maintaining stream integrity is empirically demonstrated (*sensu* Poff et al., 2010), post-construction monitoring and adaptive management may be warranted (Stein et al., 2012).

5. Summary and conclusions

Semiarid stream channels generally exhibit extreme sensitivity to hydromodification in terms of morphologic response potential and overall channel stability. As evident in this southern California case study, their sensitivity tends to increase with decreasing bed-material particle size and increasing distance from a downstream hard point. Approximately 60% of the variance in cross-sectional channel enlargement could be explained by the downstream distance to a hard point and the cumulative sediment-transport imbalance quantified over 25-yr simulations using cumulative duration histograms that were developed using mean daily flows. Models that replaced *Lr* with total impervious area were only slightly less significant but less representative of physical process.

Finally, we must reiterate that even a perfectly-matched pre-developed hydrograph over all flows does not guarantee channel stability. Rather, it only *reduces the risk* of *increased* channel instability relative to pre-developed conditions. Because most semiarid channels are inherently dynamic with natural fluxes in sediment supply and corresponding periods of aggradation, flushing, and degradation, even the best hydrologically-matched development could disrupt the sediment supply. This suggests that 'over control' of the flow regime or limiting development in upland supply zones of coarse sediment may be warranted. Furthermore, simply matching *Lr* does not address legacy effects such as historic

channelization or overgrazing. Neither does it prevent responses from poor outfall designs or headcutting from below via downstream urbanization.

Despite their uncertainties, the novel tools developed in this paper are rooted in physical understanding and calibrated with extensive regional data sets. Such regional studies provide a process-based understanding of the effects of hydromodification that shifts the management focus to the engineering-design problem; by which, innovative mitigation schemes, adaptive management, and post-construction monitoring can improve protection of downstream channel integrity as watersheds are developed.

Acknowledgements

Funding for this research was provided in part by the State of California (Water Resources Control Board Agreement No. 06-295-559-0) and San Diego County, for which we are very grateful. We also thank Eric Stein, Becky Schaffner, Liesl Tiefenthaler, Greg Lyon, and Jeff Brown of the Southern California Coastal Water Research Project (SCCWRP), and Derek Booth, Scott Dusterhoff, and Alexander Wong of Stillwater Sciences for project assistance. Dave Dust provided assistance with field data collection, bed-material data processing, and is credited with the site photographs used in this paper. Finally, we thank Chester Watson and Ellen Wohl for helpful reviews of earlier versions of this paper, and Gloria Garza for assistance with manuscript preparation. Francesco Comiti and an anonymous reviewer provided helpful comments that improved the manuscript.

Appendix A. List of symbols

A_{bf}	Bankfull cross-sectional area (m^2)
A_{post}	Surveyed cross-sectional area to top of bank (2007/2008)
A_{pre}	Best estimate of historic (reference) cross-sectional area
Ar	Enlargement expressed as the relative magnitude (m^2/m^2)
Chnlz	Binary variable representing historic channelization along reach
Cohesion	Binary variable representing relative bank cohesion
Confined	Binary variable representing valley confinement
Cp	Statistical term for Mallow's fit of a regression model that has been estimated using ordinary least squares
d_{50}	Median particle diameter
d_s	Sediment particle diameter
D_{hp}	Distance to nearest downstream hard point such as natural bedrock or artificial grade control (m)
DA	Drainage area (km^2)
DD	Drainage density, total stream length via NHD/total drainage area (km/km^2)
e	Euler's Mascheroni constant equal to approximately 2.71828
g	Acceleration of gravity
G	Specific gravity of sediment
Imp	Total impervious area as fraction of total drainage area (m^2/m^2)
L_b	Time-integrated bedload capacity (m^3)
$L_{b\text{-}bin}$	Time-integrated bedload capacity for a bin
L_{post}	Time-integrated bedload capacity from the post-developed simulations (m^3)
L_{pre}	Time-integrated bedload capacity from the pre-developed simulations (m^3)
Lr	Sediment-transport capacity load ratio between 25-yr post-developed and pre-developed DDF simulations (m^3/m^3)
n	Manning's roughness coefficient
n	Number of sites
p	Statistical term for the probability of obtaining a test statistic at least as extreme as the one that was actually observed, assuming the null hypothesis is true
q_b	Unit bedload discharge by volume (m^2/day)
$q_{b\text{-}bin}$	Unit bedload rates for each bin
q_{bv}	Unit bedload discharge by volume (m^2/day)
Q_{10}	10-Yr flow (m^3/s)
R	Hydraulic radius
R^2	Statistical term for coefficient of determination
S_f	Friction slope
S_{valley}	Valley slope (m/m)
Srf	Average surface slope of watershed (m/m)
Veg	Binary variable representing bank vegetation
VWI	Valley width index, ratio of the available valley width to the reference channel width
W_{10}	Channel top width at 10-yr flow (m)
W_{bf}	Bankfull top width (m)
W_{valley}	Valley bottom width (m)
Wr	Ratio of the post-developed top width to the pre-developed top width (m/m)
χ^2	Test statistic associated with the chi-squared distribution in which the associated *p*-value corresponds to the probability of observing a model at least as extreme as a chi-squared distribution
τ_*	Dimensionless shear stress
τ_{*c}	Shields parameter for incipient motion

References

Biedenharn, D.S., Copeland, R.R., Thorne, C.R., Soar, P.J., Hey, R.D., Watson, C.C., 2000. Effective Discharge Calculation: A Practical Guide. Technical Report TR-00-15, U.S. Army Corps of Engineers, Engineer Research and Development Center (ERDC), Coastal and Hydraulics Laboratory (CHL), Vicksburg, MS.

Biedenharn, D.S., Thorne, C.R., Soar, P.J., Hey, R.D., Watson, C.C., 2001. Effective discharge calculation guide. Int. J. Sedim. Res. 16 (4), 445–459.

Bledsoe, B.P., Brown, M.C., Raff, D.A., 2007. GeoTools: a toolkit for fluvial system analysis. J. Am. Water Resour. Assoc. 43 (3), 757–772.

Bledsoe, B.P., Stein, E.D., Hawley, R.J., Booth, D.B., 2012. Framework and tool for rapid assessment of stream susceptibility to hydromodification. J. Am. Water Resour. Assoc. 48 (4), 788–808.

Booth, D.B., 1990. Stream-channel incision following drainage-basin urbanization. Water Resour. Bull. 26 (3), 407–417.

Buhman, D.L., Gates, T.K., Watson, C.C., 2002. Stochastic variability of fluvial hydraulic geometry: Mississippi and Red Rivers. J. Hydraul. Eng. 128 (4), 426–437.

Bull, W.B., 1997. Discontinuous ephemeral streams. Geomorphology 19 (3–4), 227–276.

Bunte, K., Abt, S.R., 2001. Sampling Surface and Subsurface Particle-size Distributions in Wadable Gravel- and Cobble-bed Streams for Analyses in Sediment Transport, Hydraulics, and Streambed Monitoring. General Technical Report RMRS-GTR-74, U.S. Department of Agriculture, Forest Service, Rocky Mountain Research Station, Fort Collins, CO., 428 pp.

Bunte, K., Dust, D.D., 2008. Rigid and Flexible Procedures for Combining Volumetric Pebble Counts with Sieve Gradations by Mass. Pers. Comm.

Chien, N., 1956. The present status of research on sediment transport. Trans. Am. Soc. Civil Eng. 121, 833–868.

Chow, V.T., 1959. Open Channel Hydraulics. McGraw-Hill Book Company, Inc., New York, NY, 680 pp.

Coleman, D., MacRae, C., Stein, E.D., 2005. Effect of Increases in Peak Flows and Imperviousness on the Morphology of Southern California Streams. Technical Report #450, Stormwater Monitoring Coalition, Southern California Coastal Water Research Project, Westminster, CA, 70 pp.

County of San Diego, 2011. Hydromodification Management Plan. San Diego, CA, 294 pp.
Galster, J.C., Pazzaglia, F.J., Germanoski, D., 2008. Measuring the impact of urbanization on channel widths using historic aerial photographs and modern surveys. J. Am. Water Resour. Assoc. 44 (4), 948–960.
Graf, W.L., 1981. Channel instability in a braided sand-bed river. Water Resour. Res. 17, 1087–1094.
Graf, W.L., 1988. Fluvial Processes in Dryland Rivers. Springer-Verlag, Berlin.
Hammer, T.R., 1972. Stream channel enlargement due to urbanization. Water Resour. Res. 8, 139–167.
Harrelson, C.C., Rawlins, C.L., Potyondy, J.P., 1994. Stream Channel Reference Sites: An Illustrated Guide to Field Technique. General Technical Report RM-245, U.S. Department of Agriculture, Forest Service, Rocky Mountain Forest and Range Experiment Station, Fort Collins, CO., 61 pp.
Hawley, R.J., 2009. Effects of urbanization on the hydrologic regimes and geomorphic stability of small streams in southern California. Ph.D. Dissertation Thesis, Colorado State University, Fort Collins, CO, pp. 393.
Hawley, R.J., Bledsoe, B.P., 2011. How do flow peaks and durations change in suburbanizing semi-arid watersheds? A southern California case study. J. Hydrol. 405 (1–2), 69–82.
Hawley, R.J., Bledsoe, B.P., Stein, E.D., Haines, B.E., 2012. Channel evolution model of semiarid stream response to urban-induced hydromodification. J. Am. Water Resour. Assoc. 48 (4), 722–744.
Hey, R.D., 1997. Channel Response and Channel Forming Discharge: Literature Review and Interpretation. Final Report, U.S. Army Contract Number R&D 6871-EN-01.
Holmquist-Johnson, C.L., 2002. Computational Methods for Determining Effective Discharge in the Yazoo River Basin, Mississippi. MS Thesis, Colorado State University, Fort Collins, CO.
Julien, P.Y., 1998. Erosion and Sedimentation. Cambridge University Press, Cambridge, pp. 280.
MacRae, C.R., 1991. A Procedure for Design of Storage Facilities for Instream Erosion Control in Urban Streams. Ph.D. Thesis, University of Ottawa, Ottawa, Canada.
MacRae, C.R., 1993. An alternate design approach for the control of instream erosion potential in urban watersheds. In: Marsalek, J., Torno, H.C. (Eds.), Urban Storm Drainage: Proceedings of the Sixth International Conference, International Association for Hydraulic Research, International Association for Water Quality (IAHR/IAWQ) Joint Committee on Urban Storm Drainage, Niagra Falls, Ontario, Canada, pp. 1086–1091.
MacRae, C.R., 1997. Experience from morphological research on Canadian streams: is control of the two-year frequency runoff event the best basis for stream channel protection? In: Roesner, L.A. (Ed.), Effects of Watershed Development and Management on Aquatic Ecosystems, Proc. Engineering Conference, American Society of Civil Engineers, pp. 144–162.
Meyer-Peter, E., Müller, R., 1948. Formulas for bed-load transport. In: Proc. 2nd Meeting International Association for Hydraulic Research, Stockholm, pp. 39–64.
Montgomery, D.R., Buffington, J.M., 1997. Channel-reach morphology in mountain drainage basins. Geol. Soc. Am. Bull. 109 (5), 596–611.
Osman, A.M., Thorne, C.R., 1988. Riverbank stability analysis I: theory. J. Hydraul. Eng. 114 (2), 134–150.
Poff, N.L., Richter, B.D., Arthington, A.H., Bunn, S.E., Naiman, R.J., Kendy, E., Acreman, M., Apse, C., Bledsoe, B.P., Freeman, M.C., Henriksen, J., Jacobson, R.B., Kennen, J.G., Merritt, D.M., O'Keeffe, J.H., Olden, J.D., Rogers, K., Tharme, R.E., Warner, A., 2010. The ecological limits of hydrologic alteration (ELOHA): a new framework for developing regional environmental flow standards. Freshw. Biol. 55, 147–170.
Raff, D.A., Bledsoe, B.P., Flores, A.N., 2004. GeoTool User's Manual. Colorado State University, Fort Collins, CO.
Santa Clara Valley Urban Runoff Pollution Prevention Program, 2004. Hydromodification Management Plan Report. Sunnyvale, CA, 125 pp.
Schumm, S.A., Harvey, M.D., Watson, C.C., 1984. Incised Channels: Morphology, Dynamics, and Control. Water Resources Publications, Littleton, CO.
Smith, C.A., Sardeshmukh, P., 2000. The effect of ENSO on the intraseasonal variance of surface temperature in winter. Int. J. Climatol. 20, 1543–1557.
Soar, P.J., 2000. Channel Restoration Design for Meandering Rivers. Ph.D. Thesis, University of Nottingham, Nottingham, UK.
Stein, E.D., Federico, F., Booth, D.B., Bledsoe, B.P., Bowles, C., Rubin, Z., Kondolf, G.M., Sengupta, A., 2012. Hydromodification Assessment and Management in California. Technical Report #667, Southern California Coastal Water Research Project, Costa Mesa, CA.
Trimble, S.W., 1997. Contribution of stream channel erosion to sediment yield from an urbanizing watershed. Science 278, 1442–1444.
Watson, C.C., Dubler, D., Abt, S.R., 1997. Demonstration Erosion Control Project report. Submitted to U.S. Army Corps of Engineers, Engineer Waterways Experiment Station, Vicksburg, MS.
Wolman, M.G., Gerson, R., 1978. Relative scales of time and effectiveness of climate in watershed geomophology. Earth Surface Process. 3, 189–208.
Wolman, M.G., Miller, J.P., 1960. Magnitude and frequency of forces in geomorphic processes. J. Geol. 68, 54–74.
Wong, M., Parker, G., 2006. Reanalysis and correction of bed-load relation of Meyer-Peter and Müller using their own database. J. Hydraul. Eng. 132 (11), 1159–1168.

GIS data sources

Google Earth: Present-day Aerial Photography, earth.google.com.
National Oceanic and Atmospheric Administration (NOAA): Precipitation Intensities for 2-year, 24-hour Storm, http://www.nws.noaa.gov/oh/hdsc/ noaaatlas2.htm (Atlas 2) and hdsc.nws.noaa.gov/hdsc/pfds/pfds_gis.html (Atlas 14).
State of California Geospatial Clearinghouse (Cal-Atlas): 2000 and 2007 Roadway Shapefiles, gis.ca.gov.
U.S. Department of Agriculture (USDA), Natural Resources Conservation Service (NRCS): Soil Surveys, Average Annual Precipitation Shapefile (1961–1990), http://datagateway.nrcs.usda.gov/.
U.S. Geological Survey (USGS): Historical Aerial Photography and Quadrangle Topographic Maps, National Elevation Dataset (NED), 2001 Impervious Raster, National Hydrography Dataset (NHD), Average Annual Precipitation Shapefile (1900–1960), http://seamless.usgs.gov.